TECHNICAL ARTICLE

Improvement of X-ray stress measurement from a Debye–Scherrer ring by oscillation of the X-ray incident angle

Toshiyuki Miyazaki,[a] Yoichi Maruyama, Yohei Fujimoto, and Toshihiko Sasaki
Kanazawa Universiyt, Kanazawa city, 920-1165, Japan

(Received 26 February 2015; accepted 29 April 2015)

A technique to improve the stress measurement from a Debye–Scherrer ring (D–S ring) is reported. In a previous work, the authors reported a technique to calculate stress from the Fourier series of the normal strain of a D–S ring. That technique, similar to the cosα method that came before it, is inaccurate when the grain size of the specimen is relatively large. To cope with this problem, the authors propose using the oscillation of the X-ray incident angle. The present study demonstrates this technique to improve the stress measurement. © *2015 International Centre for Diffraction Data.*
[doi:10.1017/S0885715615000433]

Key words: X-ray stress measurement, Debye–Scherrer ring, Fourier series, X-ray incident angle oscillation

I. INTRODUCTION

Recently, a two-dimensional X-ray diffraction (XRD) technique, called the cosα method (Taira *et al.*, 1978) has enjoyed widespread commercial application. Although the cosα method can calculate the stress of a specimen from an entire Debye–Scherrer ring (D–S ring), the accuracy is significantly degraded if the grain size is relatively coarse and a sufficient number of grains are not available in the X-ray irradiation area. In such cases, the D–S ring becomes grainy and the cosα method becomes inaccurate (Sasaki *et al.*, 1997) even if the specimen is under a plane stress condition. With the $\sin^2\psi$ method (for example see Noyan and Cohen, 1987), a commonly used conventional XRD method, the oscillation of the X-ray incident angle has been used to measure the stress of a coarse-grained specimen. Maruyama proposed using the X-ray incident angle oscillation with the cosα method (Maruyama).

The authors, previously proposed a generalization of the cosα method based on Fourier analysis (Miyazaki and Sasaki, 2014), and demonstrated that it could determine the stress of a carbon steel specimen. The purpose of the present study is to demonstrate that the X-ray incident angle oscillation improves the stress measurement of this method when measuring a coarse-grained specimen. Additionally, a primitive compensation for the X-ray incident angle oscillation is proposed.

II. PRINCIPLE

A. Fourier analysis of the D–S ring

In this section, the stress measurement from a D–S ring is briefly summarized. The arrangement of the stress measurement as laid out by Miyazaki and Sasaki (2014) is shown in Figure 1. If the specimen is under the plane stress, the normal strain along the direction of the circumference angle α of the D–S ring is

$$\varepsilon(\alpha) = a_0 + a_1\cos\alpha + b_1\sin\alpha + a_2\cos 2\alpha + b_2\sin 2\alpha \quad (1)$$

The constant term a_0 does not affect the following discussion and is thus omitted. From here, we refer to Eq. (1) as the "plane stress approximation". Each coefficient of Eq. (1) is related to the stress of the specimen using Young's modulus E and Poisson's ratio ν as

$$\begin{aligned} a_1 &= -\frac{1+\nu}{2E}\sin 2\eta\sin 2\psi_0\cdot\sigma_x \\ b_1 &= \frac{1+\nu}{E}\sin 2\eta\sin\psi_0\cdot\tau_{xy} \\ a_2 &= \frac{1+\nu}{2E}\sin^2\eta(\cos^2\psi_0\sigma_x-\sigma_y) \\ b_2 &= -\frac{1+\nu}{2E}\sin^2\eta\cos\psi_0\cdot\tau_{xy} \end{aligned} \quad (2)$$

where η is the complement of the diffraction angle θ ($\eta=\pi/2-\theta$), ψ_0 is the angle between the sample surface normal and the X-ray incident angle, and, σ_x, σ_y, and τ_{xy} are the longitudinal stress, the lateral stress, and the shear stress, respectively. Please note that ψ_0 differs from ψ which traditionally represents the inclination angle of the specimen surface normal with respect to the diffraction vector (For example, see Figure 1 in Welzel *et al.*, 2005). To simplify, we call ψ_0 as "X-ray incident angle" or "incident angle" in the following discussion. The stress of the specimen can be calculated from Eq. (2).

[a]Author to whom correspondence should be addressed. Electronic mail: trmiyazaki@staff.kanazawa-u.ac.jp

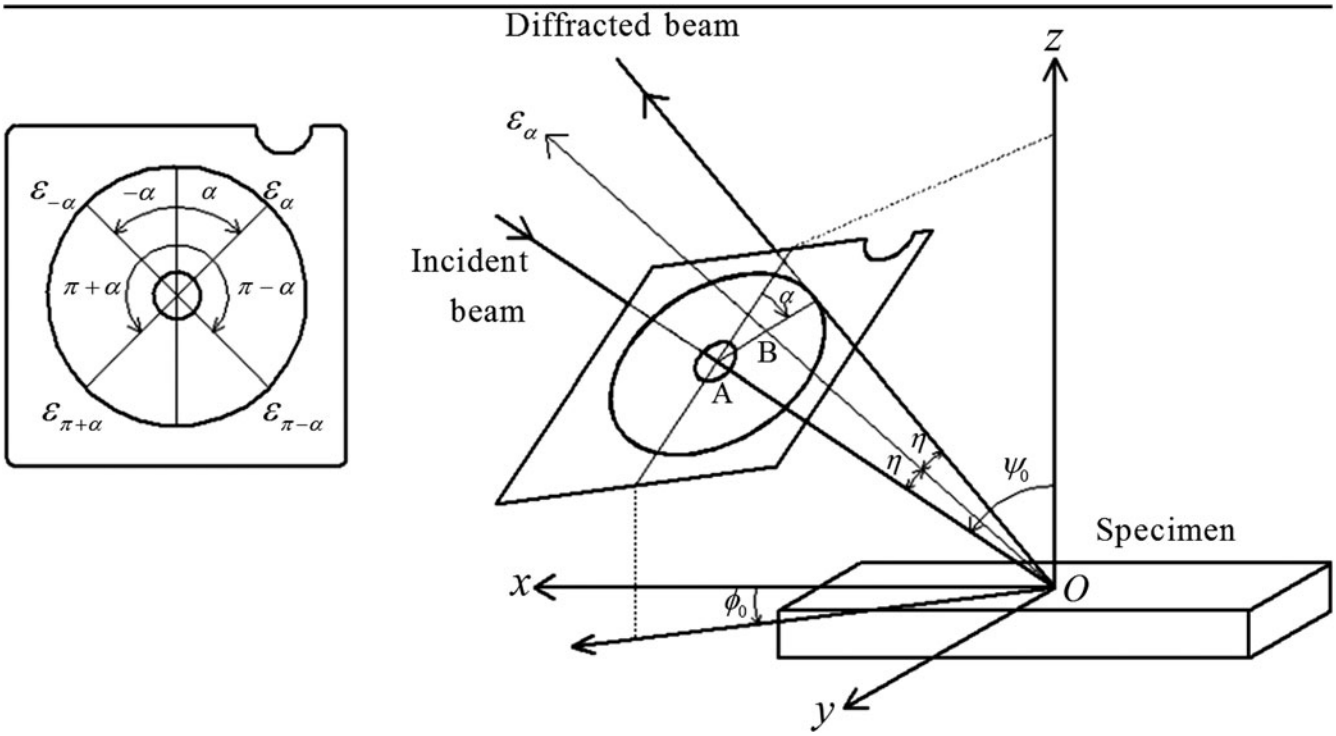

Figure 1. Arrangement of the stress measurement [from Miyazaki and Sasaki (2014)].

For example,

$$\sigma_x = -\frac{2E}{1+\nu}\frac{1}{\sin 2\eta \sin 2\psi_0}\cdot a_1$$
$$\tau_{xy} = \frac{E}{1+\nu}\frac{1}{\sin 2\eta \sin \psi_0}\cdot b_1 \quad (3)$$

The reader may think that our method is similar to the φ-integral method (Lode and Peiter, 1981). A good summary can be found in Welzel *et al.* (2005). However, the authors consider that the two methods to be entirely different (Miyazaki and Sasaki, 2015).

B. Oscillation of the X-ray incident angle

Even if the specimen is under plane stress in the macroscopic scale (>∼mm), the residual stress varies over the grain scale. Consequently, the D–S ring becomes rough and $\varepsilon(\alpha)$ becomes as

$$\varepsilon(\alpha) = a_0 + a_1\cos\alpha + b_1\sin\alpha + a_2\cos 2\alpha + b_2\sin 2\alpha + \delta\varepsilon(\alpha) \quad (4)$$

where $\delta\varepsilon(\alpha)$ represents the effect of the residual stress over the grain scale and contains higher order components (cos3α, sin3α, cos4α, sin4α, and so on). For most applications, it is desirable to know the macroscopic plane stress values of the specimen and $\delta\varepsilon(\alpha)$ can be regarded as the measurement noise. In order to reduce the influence of $\delta\varepsilon(\alpha)$ on the cosα method, Maruyama proposed oscillating the X-ray incident angle ψ_0 (Maruyama) (Figure 2). In this study, we report on the effect of ψ_0 oscillation with the Fourier series analysis proposed by Miyazaki and Sasaki (2014).

The Fourier coefficients of Eq. (2) depend on ψ_0, so it is necessary to compensate for the effect of the incident angle oscillation. In the following, we consider the compensation for the simplest case.

When the incident angle is ψ (this ψ is the angle between the sample surface normal and the X-ray incident angle), Eq. (2) can be modified as

$$\varepsilon(\alpha,\psi) = a_1(\psi)\cos\alpha + b_1(\psi)\sin\alpha + a_2(\psi)\cos 2\alpha + b_2(\psi)\sin 2\alpha \quad (5)$$

where $a_1(\psi)$ to $b_2(\psi)$ are the functions of ψ. From Eq. (2), $a_1(\psi)$ to $b_2(\psi)$ can be described as

$$a_1(\psi) = -\frac{1+\nu}{2E}\sin 2\eta \sin 2\psi\cdot\sigma_x$$
$$b_1(\psi) = \frac{1+\nu}{E}\sin 2\eta \sin\psi\cdot\tau_{xy}$$
$$a_2(\psi) = -\frac{1+\nu}{2E}\sin^2\eta\cdot\sigma_y + \frac{1+\nu}{2E}\sigma_x\sin^2\eta\cos^2\psi \quad (6)$$
$$b_2(\psi) = -\frac{1+\nu}{2E}\sin^2\eta\cos\psi\cdot\tau_{xy}$$

Next, we consider the effect of the ψ oscillation on $\varepsilon(\alpha)$. In order to simplify, we assume that when ψ moves from $\psi_0-\delta$ to $\psi_0+\delta$, the D–S ring is observed as the simple average on ψ as

$$\bar{\varepsilon}(\alpha) = \frac{1}{2\delta}\int_{\psi_0-\delta}^{\psi_0+\delta}\varepsilon(\alpha,\psi)d\psi \quad (7)$$

with this assumption, Eq. (5) becomes

$$\bar{\varepsilon}(\alpha) = \bar{a}_1\cos\alpha + \bar{b}_1\sin\alpha + \bar{a}_2\cos 2\alpha + \bar{b}_2\sin 2\alpha \quad (8)$$

https://doi.org/10.1017/S0885715615000433 Published online by Cambridge University Press

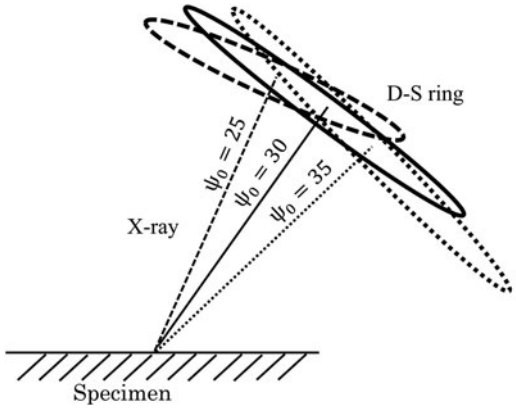

Figure 2. Schematic of the X-ray incident angle oscillation.

where

$$\bar{x} = \frac{1}{2\delta}\int_{\psi_0-\delta}^{\psi_0+\delta} x(\psi)d\psi \quad (x = a_1,\ b_1,\ a_2 \text{ and } b_2) \tag{9}$$

Applying Eq. (9) to Eq. (6) and developing up to δ^2 terms, we obtain

$$\begin{aligned}
\bar{a}_1 &= a_1(\psi_0)\cdot\left(1-\frac{2}{3}\delta^2\right)\\
\bar{b}_1 &= b_1(\psi_0)\cdot\left(1-\frac{1}{6}\delta^2\right)\\
\bar{a}_2 &= a_2(\psi_0) - \frac{1+\nu}{6E}\sigma_x \sin^2\eta\cos 2\psi_0\cdot\delta^2\\
\bar{b}_2 &= b_2(\psi_0)\cdot\left(1-\frac{1}{6}\delta^2\right)
\end{aligned} \tag{10}$$

Consequently, when applying the incident angle oscillation, compensations according to Eq. (10) are required.

For example, Eq. (3) becomes

$$\begin{aligned}
\sigma_x &= -\frac{2E}{1+\nu}\frac{1}{\sin 2\eta\sin 2\psi_0}\cdot\bar{a}_1\cdot\left(1+\frac{2}{3}\delta^2\right)\\
\tau_{xy} &= \frac{E}{1+\nu}\frac{1}{\sin 2\eta\sin\psi_0}\cdot\bar{b}_1\cdot\left(1+\frac{1}{6}\delta^2\right)
\end{aligned} \tag{11}$$

when $\delta = 5°$, the compensation of σ_x is ~0.5% and when $\delta = 10°$, the compensation of σ_x and τ_{xy} are ~2% and ~0.5%, respectively.

III. EXPERIMENT

We tested the proposed technique with a carbon steel specimen. The specimen was made of JIS-S40C and measured 150 mm long, 20 mm wide and 3 mm thick. In order to remove the residual stress, the specimen was annealed for 20 min at 600 °C in an Ar atmosphere. Figure 3 shows a micrograph of the specimen, where the grain size is approximately 10 μm. A 20 mm × 20 mm area was electropolished 150 μm deep to remove the effect of surface processing. The following X-ray measurements were then applied to this part.

Prior to the measurement with the new method, we applied four-point bending tests and measured X-ray stress by means of the $\sin^2\psi$ method with a Rigaku MSF-2M stress analyzer

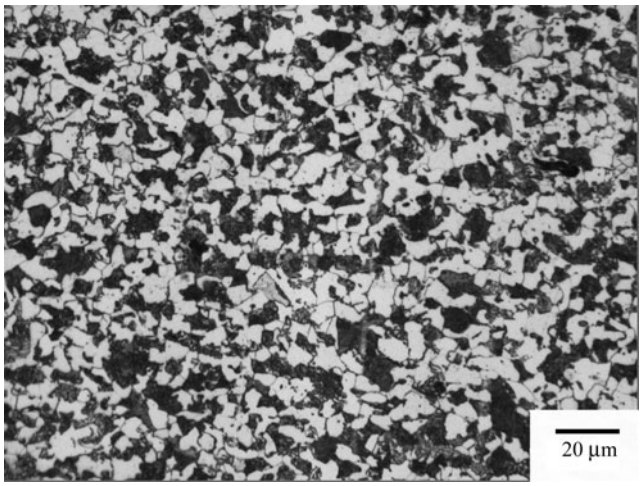

Figure 3. Micrograph of the specimen (JIS-S40C).

using 211 reflection of Cr$K\alpha$ line. From the measurement, we determined the X-ray elastic constant of the specimen as

$$\frac{E}{1+\nu} = 186 \quad \text{(GPa)}$$

In addition, we confirmed that the shear stress of the specimen was

$$\tau_{xy} \sim 0 \tag{12}$$

We applied a four-point bending test on the specimen while measuring the D–S ring with a μ-X360 X-ray stress measurement instrument provided by Pulstec Industrial (Pulstec). The characteristic X-ray used, Cr$K\alpha$, was irradiated through a 1-mmϕ collimator. Throughout the study, the distance between the specimen and the imaging detector was approximately 39 mm and the radius of each D–S ring was approximately 17 mm. Obtained D–S rings were treated by standard processing with the instrument software. Other measurement conditions were set according to Miyazaki and Sasaki (2014).

In order to apply the incident angle oscillation, we oscillated the μ-X360 with a gonio stage provided by Pulstec Industrial. Figure 4 shows the entire measurement system. In the following experiment, the center of the X-ray incident

Figure 4. X-ray stress analyzer and the gonio stage.

https://doi.org/10.1017/S0885715615000433 Published online by Cambridge University Press

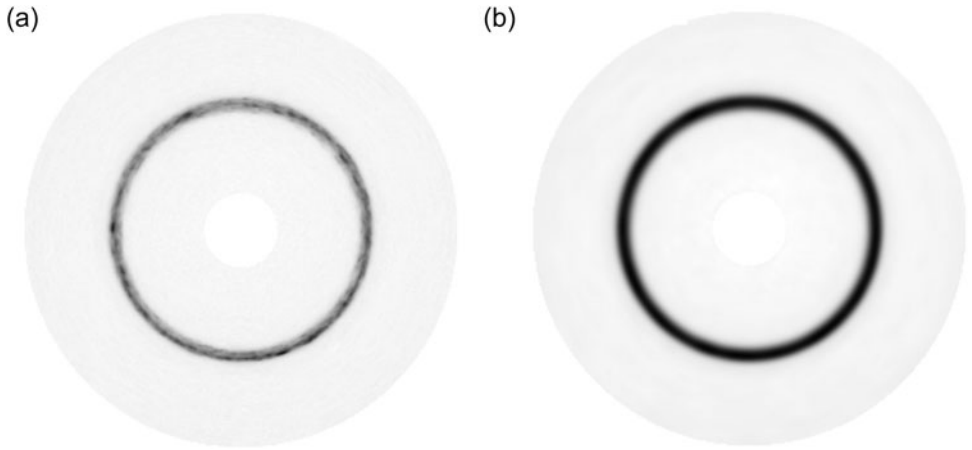

Figure 5. Examples of measured D–S rings (stress applied ~160 MPa). (a) Without the incident angle oscillation. (b) With ±10° oscillation.

angle was set to $\psi_0 = 25°$ and ±5° or ±10° oscillations were applied. The X-ray exposure time was 30 s throughout this study and the ψ was moved so as to satisfy the assumption of Eq. (8).

Figure 5(a) shows an example of a D–S ring obtained without the oscillation. From this D–S ring, $\varepsilon(\alpha)$was obtained (Figure 6). In this example, stress of approximately 160 MPa was applied to the specimen. Compared with the plane stress assumption (dashed line, described later), $\varepsilon(\alpha)$ in the figure contains relatively large $\delta\varepsilon(\alpha)$, and the estimations of the macro stress values are likely to have a large number of errors.

Next, we applied the incident angle oscillation [Figure 5(b) shows an example of D–S ring] and obtained $\varepsilon(\alpha)$ (Figures 7 and 8). The oscillation angles δ were ±5° (Figure 7) and ±10° (Figure 8). From these figures, we can state that the incident angle oscillation reduces the effect of $\delta\varepsilon(\alpha)$. These effects made little difference for $\delta = \pm 5°$ and $\delta = \pm 10°$.

We assumed that the $\varepsilon(\alpha)$ of Figure 8 was a good approximation of the macro stress of the specimen and calculated the Fourier coefficients $\bar{a}_1$, $\bar{b}_1$, $\bar{a}_2$, and $\bar{b}_2$. We applied the compensation of Eq. (10) and obtained the plane stress approximation as

$$\varepsilon(\alpha) = a_1(\psi_0)\cos\alpha + b_1(\psi_0)\sin\alpha + a_2(\psi_0)\cos 2\alpha + b_2(\psi_0) \times \sin 2\alpha$$

In order to examine the effect of the incident angle oscillation, we calculated the power spectrum of $\varepsilon(\alpha)$ (Figure 9). In this plot, the horizontal axis represents k from the Fourier series of $\varepsilon(\alpha)$

$$\varepsilon(\alpha) = \sum_{k=1}^{\infty}(a_k \cos k\alpha + b_k \sin k\alpha)$$

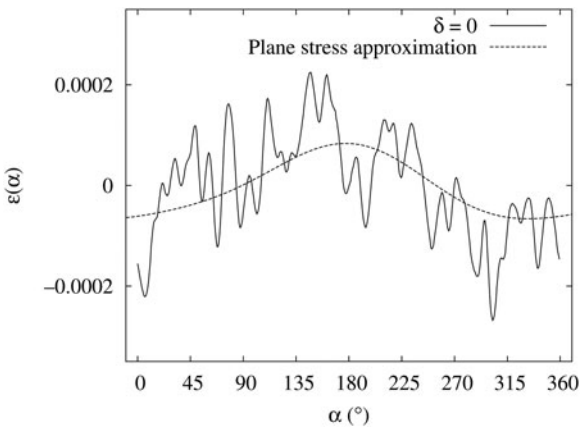

Figure 6. $\varepsilon(\alpha)$ from the D–S ring of Figure 5 (solid line) and the plane stress approximation (dashed line).

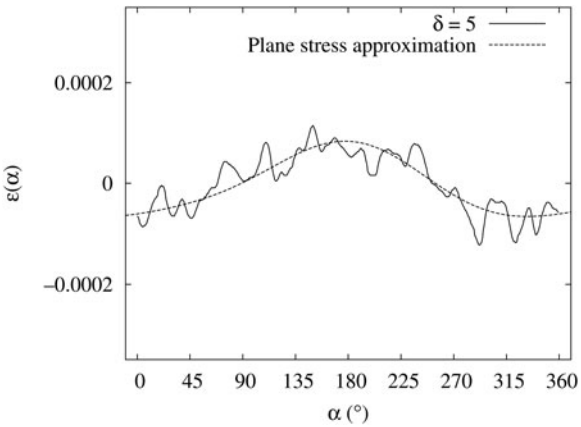

Figure 7. $\varepsilon(\alpha)$ with ±5° incident angle oscillation (solid line) and the plane stress approximation (dashed line) (stress applied ~160 MPa).

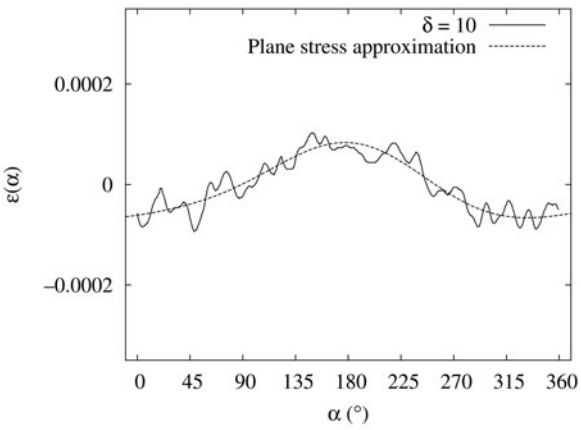

Figure 8. $\varepsilon(\alpha)$ with ±10° incident angle oscillation (solid line) and the plane stress approximation (dashed line) (stress applied ~160 MPa).

https://doi.org/10.1017/S0885715615000433 Published online by Cambridge University Press

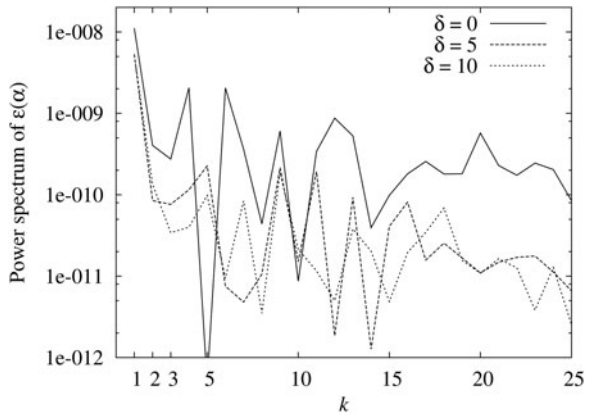

Figure 9. Power spectrum of $\varepsilon(\alpha)$ (stress applied ~160 MPa). Without the incident angle oscillation ($\delta = 0$), with ±5° oscillation ($\delta = 5$), and with ±10° oscillation ($\delta = 10$).

The vertical axis represents the power spectrum of $\varepsilon(\alpha)$:

$$E(k) = a_k^2 + b_k^2$$

The plane stress components appear only at $k = 1$, 2, and $k \geq 3$ components are produced by $\delta\varepsilon(\alpha)$. From Figure 9, it can be observed that the incident angle oscillation reduces the power spectrum at $k \geq 3$. This is because the oscillation reduces the effect of $\delta\varepsilon(\alpha)$. Moreover, $E(1)$ and $E(2)$ are also affected by $\delta\varepsilon(\alpha)$. Consequently, the macro stress values estimated without the ψ oscillation contain a relatively large number of errors because of $\delta\varepsilon(\alpha)$.

It is also possible to estimate the error of the stress because of $\delta\varepsilon(\alpha)$. From Figure 9, it can be seen that the non-plane-stress components of *E(k)* have a small dependence on k and can be regarded as white noise. Therefore, the errors of the plane stress components a_1–b_2 by the $\delta\varepsilon(\alpha)$ can be estimated as

$$\delta a_1 \sim \delta b_1 \sim \delta a_2 \sim \delta b_2 \sim \sqrt{\frac{E(3)}{2}} \sim \sqrt{\frac{E(4)}{2}} \cdots \qquad (13)$$

Next, we measured D–S rings with and without the incident angle oscillation while applying a four-point bending test to the specimen. Figure 10 shows the result without the incident angle oscillation and Figure 11 that with ±10° oscillation. In both figures, the horizontal axis shows the applied mechanical stress and the vertical axis shows the stress by X-ray [Eq. (3)]. The errors of a_1 and b_1 (discussed later) are calculated using the average of E (3)~E (5) and Eq. (13) as

$$\delta a_1 \sim \delta b_1 \sim \sqrt{\frac{E(3) + E(4) + E(5)}{2 \times 3}}$$

In both figures, the X-ray measured stresses are proportional to the mechanically applied stress and the proportional coefficients are close to 1.0 (0.98 and 1.00, respectively). The error bars are smaller with the incident angle oscillation and the fitted lines are within a 95% confidence range from the measured σ_x.

Figure 12 shows the X-ray measured τ_{xy} calculated from b_1 using Eq. (3). The horizontal axis shows the mechanically applied stress to the specimen. The solid error bars represent τ_{xy} from the measurement without the incident angle oscillation and the dashed error bars represent those with ±10° oscillation. The averaged τ_{xy} were

$$\tau_{xy} = 54 \quad \text{(MPa) (without oscillation)}$$

$$\tau_{xy} = 10 \quad \text{(MPa) (with } \pm 10^\circ \text{ oscillation)}$$

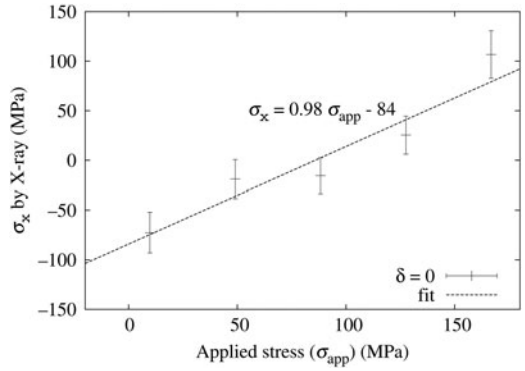

Figure 10. Stress applied with a four-point bending test (horizontal axis) and the X-ray measured stress σ_x without the incident angle oscillation (vertical axis).

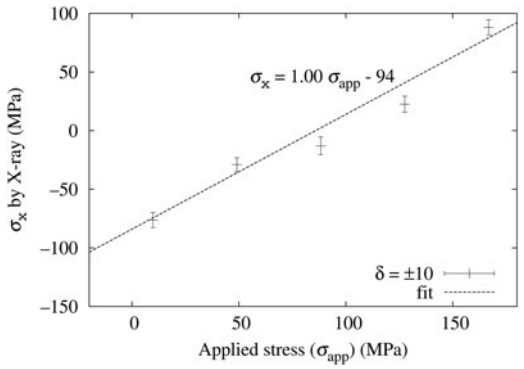

Figure 11. Stress applied with a four-point bending test (horizontal axis) and the X-ray measured stress σ_x with ±10° incident angle oscillation (vertical axis).

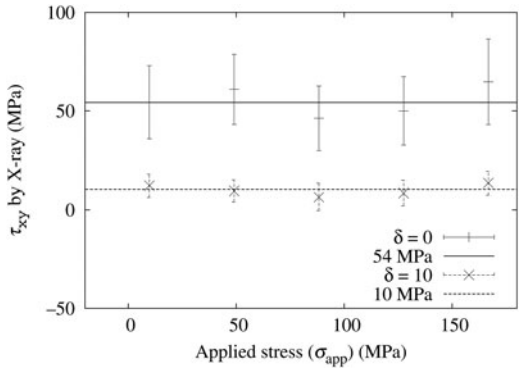

Figure 12. Stress applied with a four-point bending test (horizontal axis) and the X-ray measured shear stress τ_{xy}. Without the incident angle oscillation ($\delta = 0$) and with ±10° oscillation ($\delta = 10$).

https://doi.org/10.1017/S0885715615000433 Published online by Cambridge University Press

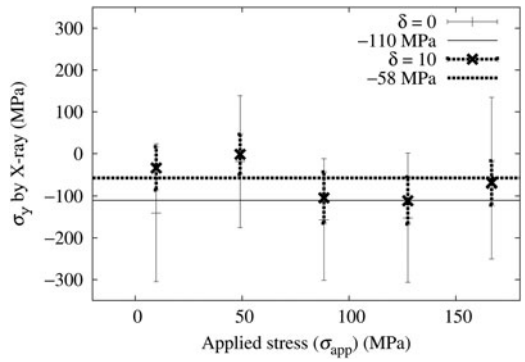

Figure 13. Stress applied with a four-point bending test (horizontal axis) and the X-ray measured stress σ_y. Without the incident angle oscillation ($\delta = 0$) and with ±10° oscillation ($\delta = 10$).

A comparison with Eq. (12) leads us to conclude that the incident angle oscillation of XRD system provides more accurate value.

In this study, the τ_{xy} value was improved by the ψ oscillation while the improvement of the σ_x value was not clear. This is because the $\delta\varepsilon(\alpha)$ of this experiment contains more of a $\sin\alpha$ component than a $\cos\alpha$ component.

Figure 13 shows the X-ray measured σ_y calculated from a_1 and a_2 using Eq. (2). The horizontal axis shows the mechanically applied stress to the specimen. The solid error bars represent σ_y from the measurement without the incident angle oscillation and the dashed error bars represent those with ±10° oscillation. Eq. (10) was used to compensate the oscillation. The averaged σ_y were

$$\sigma_y = -110 \quad \text{(MPa) (without oscillation)}$$

$$\sigma_y = -58 \quad \text{(MPa) (with } \pm 10^{\circ}\text{oscillation)}$$

Although both measurements agree with $\sigma_y = 0$ within the 95% confidence range (two times of the error bars of Figure 13), estimation errors are large compared with σ_x and τ_{xy} cases. Further improvements are required to the σ_y estimation.

IV. CONCLUSION

In this paper, we applied incident angle oscillation to an X-ray stress measurement by Fourier analysis of a D–S ring. Incident angle oscillation is effective with coarse-grained specimens producing a grainy D–S ring. The proposed technique makes the normal strain $\varepsilon(\alpha)$ closer to the plane stress approximation. This effect was clearly illustrated by the power spectrum of $\varepsilon(\alpha)$. Although the improvement to σ_x values was not clear, we did find that the τ_{xy} values were significantly improved. We also proposed a method to estimate the measurement errors by the grain scale stress from the power spectrum. The estimations seem to be consistent with the measurements of this study.

The effective incident angle of the D–S ring obtained with the incident angle oscillation differs from the center of the oscillation angle ψ_0. We estimated this effect for the simplest case and found that at less than 2% for ±10° oscillation, it is not significant in terms of actual stress measurement.

ACKNOWLEDGMENTS

This work was partially supported by a Grant-in-Aid for the Innovative Nuclear Research and Development Program (No. 120804) from the Ministry of Education, Culture, Sports, Science and Technology in Japan.

Lode, W. and Peiter, A. (**1981**). "X-ray-measurable deformations in superficial layers and their representations," Materialpruefung **23**, 227–230.

Maruyama, Y. *Ph.D thesis,* Kanazawa University (In progress, 2015).

Miyazaki, T. and Sasaki, T. (**2014**). "X-ray stress measurement with two-dimensional detector based on Fourier analysis," Int. J. Mater. Res. **105**, 922–927.

Miyazaki, T. and Sasaki, T. (**2015**). "X-ray stress measurement from an imperfect Debye–Scherrer ring," Int. J. Mater. Res. **106**, 3:237–241.

Noyan, I. C. and Cohen, J. B. (**1987**). *Residual Stress* (Springer-Verlag, New York).

Sasaki, T., Hirose, Y., and Yasukawa, S. (**1997**). "X-ray stress measurement of coarse-grained polycrystalline materials by imaging plate method," Trans. Jpn. Soc. Mech. Eng. Part A. **63**, 533–541.

Taira, S., Tanaka, K., and Yamasaki, T. (**1978**). "A method of x-ray microbeam measurement of local stress and its application to fatigue crack growth problem," J. Soc. Mat. Sci, Japan. **27**, 251–256.

Welzel, U., Ligot, J., Lamparter, P., Vermeulen, A. C., and Mittermeijer, E. J. (**2005**). "Stress analysis of polycrystalline thin films and surface regions by X-ray diffraction," J. Appl. Crystallogr. **38**, 1–29.

https://doi.org/10.1017/S0885715615000433 Published online by Cambridge University Press